Vorinostat Reverses Paclitaxel Resistance Induced by SIRT6 Upregulation Through Enhancing Autophagy in Lung Cancer

Dongfang Tang
Huadong Hospital Affiliated to Fudan University
Jing Wang
Huadong Hospital Affiliated to Fudan University
Yifeng Sun
Shanghai Chest Hospital: Shanghai Jiao Tong University Affiliated Chest Hospital
Liming Lu
Shanghai Chest Hospital: Shanghai Jiao Tong University Affiliated Chest Hospital
Wen Gao (gaowenchest@163.com)
Huadong Hospital Affiliated to Fudan University https://orcid.org/0000-0003-0893-5081

Research Article

Keywords: Lung squamous cell carcinoma, SIRT6, vorinostat, autophagy, TGF-β

Posted Date: January 24th, 2022

DOI: https://doi.org/10.21203/rs.3.rs-1251650/v1

Abstract

Background

Major obstacle to improve the lung squamous cell carcinoma (L-SCC) patients' prognosis is the acquired chemoresistance.

Materials and methods

we investigated the clinical significance of *SIRT6*, which plays a key role in the resistance to paclitaxel-based chemotherapy. Firstly, we detected the expression and localization of SIRT6, then explored the inhibitory effect of histone deacetylase inhibitor (vorinostat) on paclitaxel-resistant squamous cell carcinoma cell lines, and determined the role of autophagy in reversing the paclitaxel-resistance induced by *SIRT6* upregulation.

Results

SIRT6 improved significantly in L-SCC patients than that in lung adenocarcinoma (L-AD); the expression of *SIRT6* was higher in advanced stage patients than in early stage (P<0.001); finally we found that *SIRT6* might promote paclitaxel resistance via upregulating TGF-β; and vorinostat could reverse paclitaxel resistance in L-SCC through enhancing autophagy.

Conclusion

SIRT6 might be one useful prognostic biomarker and represent a novel target to overcome the chemoresistant L-SCC patients.

Introduction

The chemotherapeutic regimens are less for lung squamous cell carcinoma (L-SCC) patients compared with lung adenocarcinoma(L-AD) ones, there are only several options, of which cisplatin plus paclitaxel (TP) regimen is the most common.[1,2] However, taxol-resistance occurred frequently in clinic, and how to carry subsequent treatments after taxol-resistance still is one challenge.

Sirtuins (SIRTs) is one highly conserved family of NAD^+- dependent deacetylases.[3] SIRT family members are believed to play distinct roles in tumorigenesis. *SIRT6*, locating on a chromosomal locus (19p13.3) that is a frequent breakage site in human acute myeloid leukemia,[4,5] is over-expressed in several cancers, including prostate,[6] endometrioid carcinomas, and keratinocyte-derived skin squamous cell carcinomas.[7] Furthermore, it reported that *SIRT6* was down-regulated in pancreatic cancer,[8] hepatocellular carcinoma

(HCC)[9,10] and colorectal carcinoma.[11] However, in HCC,over-expressed *SIRT6* could inhibit HCC cell growth. In breast cancer, high nuclear expression of *SIRT6* might predict poor prognosis.[12,13] *SIRT6* also enhanced sensitivity to radiation damage and reduced cell viability in lung cancer.[14] Therefore, the role of *SIRT6* in cancers was complicated. In previous study, we found that *SIRT6* was highly expressed in L-SCC than L-AD, indicating its association with taxol-resistance.

HDAC inhibitors (HDACi) have been identified as potential anticancer agents. Histones comprise the protein core of nucleosomes and their modification by acetylation and/or deacetylation affects chromatin structure and regulates gene expression.[15] Drugs that function as HDAC inhibitors are hypothesized to induce differentiation, cause growth arrest and promote apoptosis. It is reported that vorinostat (SAHA) increases carboplatin and paclitaxel activity in non-small-cell lung cancer (NSCLC) cells;[16] and SAHA potentiates paclitaxel-induced apoptosis in ovarian cancer cell lines.[17] In addition, it has demonstrated that SAHA and paclitaxel could cause synergistic effects on apoptosis and microtubule stabilization in papillary serous endometrial cancer cells.[18]

In present study, we intended to demonstrated: a) the relationship between *SIRT6* and taxol-resistance in L-SCC; b) the molecular mechanism of taxol-resistance induced by *SIRT6* upregulation in L-SCC; c) illuminated the anticancer effect of SAHA on taxol-resistance in L-SCC; d) analyzed the role of autophagy in reversing taxol-resistance in the lung cancer.

Materials And Methods

All experimental protocols were approved by our local quality committee, and were carried out in accordance with our institutional guidelines.

Human Samples

Human lung cancer and corresponding non-cancer tissues were collected at the time of resection from 64 patients with NSCLC from May 2017 to June 2018 at the department of thoracic surgery in HuaDong hospital affiliated to FuDan University. Tissues were frozen in liquid nitrogen and stored at -80℃ refrigerator immediately. Patients who relapsed within 3 months after the first course of chemotherapy were defined as chemoresistance; ≥3 months was sensitive.

The signed informed consent was obtained from all patients and the clinical research ethics committee of FuDan university approved the present study.

Cell Culture And Regents

The NSCLC cell lines (SW900, SW900-Taxol) were purchased from the Cell Resource Center, Shanghai Institute of Biochemistry and Cell Biology at the Chinese Academy of Sciences. SW900-Taxol cell line

refers to paclitaxel-resistant SW900 cell line. Both cells were maintained at 37°C in humidified air atmosphere containing 5% carbon dioxide in RPMI 1640 supplemented with 10% FBS. Rapamycin (R0395) and chloroquine (C6628) were purchased from Sigma; vorinostat (SAHA) was purchased from Selleck (Houston, TX, USA) and dissolved in dimethylsulfoxide (DMSO) as 10 mmol/L stock solutions.

RNA extraction and quantitative real-time PCR

Total RNA was extracted from cultured cells using the Isolation Kit (Ambion; Life Technologies), RNA was extracted from formalin-fixed/paraffin-embed normal and lung cancer specimens using the Recover All Total Nucleic Acid Isolation Kit (Ambion; Life Technologies). cDNA was synthesized from total RNA with specific stem-loop primers and the TaqMan Reverse Transcription Kit (Applied Biosystems; Life Technologies).

The sequences of the primers were as follows:

SIRT6, forward, 5'-CCCACGGAGTCTGGACCAT -3';

Reverse, 5'- CTCTGCCAGTTTGTCCCTG -3';

TGF-β, forward: 5'- GGCCAGATCCTTCCAAGC -3',

Reverse: 5'-GTGGGTTTCCACCATTAGCAC -3';

GAPDH was used as an internal control and amplified with forward primer: 5'-GGAGCGAGATCCCTCCAAAAT-3',

Reverse primer: 5'-GGCTGTTGTCATACTTCTCATGG-3'.

Western Blot Analysis

According to the standard procedure, proteins were separated by 8% SDS-PAGE and transferred to nitrocellulose membrane (Bio-Rad). After blocked in 5% non-fat milk, the membranes were incubated with the primary antibodies: rabbit anti-SIRT6 and anti-TGF-β monoclonal antibody (mAb; 1:1000; CST), rabbit anti-β-Actin mAb (1: 1000; CST). The proteins were visualized with enhanced electrochemiluminescence (ECL) agents (Pierce).

Migration And Invasion Assay

For transwell migration assays, 2.5×10^4 to 5×10^4 cells were plated in the top chamber with the non-coated membrane (24-well insert; pore size, 8 um; BD Biosciences). For invasion assays, 1.25×10^5 cells were plated in the top chamber with matrigel coated membrane (24-well insert; pore size, 8 um; BD

Biosciences). In both assays, cells were plated in medium without serum or growth factors, and medium which supplemented with growth factors or serum was used as a chemo-attractant in the lower chamber. The cells were incubated for 24 h and cells that did not migrate or invade through the pores were removed by a cotton swab. Cells on the lower surface of the membrane were stained with the Crystal Violet (GuangZhou Xilong Chemical industry co.) and counted.

Immunohistochemistry

The resected tissues were fixed with 10% formaldehyde, embedded in paraffin blocks. All sections were incubated at 63°C for 60 mins, deparaffinized in xylene, rehydrated, and incubated with fresh 0.3% hydrogen peroxide in 100% methanol for 30 mins at 37°C to block endogenous peroxidase activity. After rehydration through a graded ethanol series, antigen retrieval was carried out in 10 mM citrate buffer (pH6.4) at 98°C–100°C for 20 mins.The sections were passively cooled to 30°C. After rinsing the sections in 0.1M phosphate - buffered saline (pH7.4), non-specific binding sites were blocked by incubating with 10% normal goat serum for 30 mins. The sections were incubated overnight at 4°C or 37°C for 30 mins with anti-SIRT6 antibodies (CST) at a dilution of 1:100 in PBST. The sections were washed using PBST, incubated with biotinylated anti-mouse IgG, A, M solution (NichireiCo., Tokyo, Japan) for 30 mins at 37°C, and finally incubated in S-ABC solution (Nichirei Co.) for 30 mins. The chromogen, 3,3’-diaminobenzidine tetrahydrochloride, was applied as a 0.02% solution containing 0.005% hydrogen peroxide in a 50 mM ammonium acetate-citrate acid buffer (pH6.0).

The sections were counterstained in Mayer’s hematoxylin and mounted on glass slides. The expression levels were defined as follows:(1) low expression: no staining, weak staining or strong complete cytoplasm/ nuclear staining in <20% of tumor cells; (2) high expression/strong complete cytoplasm/nuclear staining in ≥20% of tumor cells. The expression levels were evaluated by two independent investigators who reached a consensus for all samples.

Immunofluorescence (IF)

Cells were fixed with 4% formaldehyde, permeabilized with 0.4% Triton, and blocked with 2% BSA. The cells were stained with anti-SIRT6 (1:100), anti-LAMP2 (1:100), anti-LC3 (1:100) at 4°C. In the next day, the cells were incubated with FITC-conjugated secondary antibody for 1 h, and observed under a fluorescence microscope. To label the nuclei, cells were counterstained with 4’, 6-diamidino-2-phenylindole (DAPI, Invitrogen) and were visualized using a confocal microscope.

Microscopy

Cells were plated at low con□uence in 12-well plates ($5*10^4$ cells/well). On the 2 day, cells were exposed to serum starvation (0% FBS), normal medium (10% FBS), Rapamycin (30 umol/L), chloroquine (50

mmol/L) and SAHA for 24 hours. Medium was removed, cells were washed with PBS and treated with 4% paraformalde hyde/PBS for 20 minutes at room temperature, washed, and permeabilized with 0.1% Triton X-100 for 10 mins. Cells were blocked with 5% normal goat serum (CST) containing 0.4% Triton X-100 in PBS for 60 mins. Diluted primary antibody, anti-mouse LC3 A/B (CST), was applied in blocking buffer overnight at 4℃. Alexa Fluor-555 secondary antibodies diluted in 1% normal goat serum in PBS were added for 1 hour at ambient temperature. Cells were xed using Vectashield hard set mounting medium containing DAPI dye (Vector Laboratories). Images were acquired using confocal microscopy (Olympus FV-1000) and overlaid using ImageJ.

Cell Viability Assays

Cells were seeded in 96-well plates ($1*10^3$–$3*10^3$ cells per well depending on the cell type) and incubated overnight before treatment. Cell viability was measured using the CellTiter 96® AQueous MTS Reagent (Promega, Madison, WI). For Giemsa staining, cells were washed with PBS and fixed with formaldehyde and washed again before incubation with Giemsa staining solution (Sigma, St Louis, MO). After 30 mins, cells were washed and allowed to dry. Each subgroup has three holes.

Flow cytometry after annexin-V/propidium iodide (PI) staining

The collected cells were centrifuged at 2000 rpm/min for 5 min, and the centrifuged cells were washed twice with PBS. The washed cells were centrifuged and collected, and the treated cells ($1*10^6$) were transferred into an Ependorff (EP) tube and 500 μL of bidding buffer was added into EP tube. PI (5 μL) and Annexin V (5 μL) (KeyGEN BioTECH, Nanjing, China) were added into each EP tube. After the dyes were added, the cells were incubated in the dark for 10-15 mins. The incubated cell suspension was filtered through 400 mesh cell screen to filter off the cell clumps. After filtration, the cells were placed on ice and analyzed within 30 mins using flow cytometer. Annexin V^+PI^- indicated early apoptosis, Annexin V^+ PI^+ indicated late apoptosis. Apoptotic rate = early + late apoptosis rates.

Statistical analysis

Data were shown as mean±SD, the student-t test was used for statistical analysis; all statistical analyses were performed with the SPSS 22.0 software. The Cox regression method was adopted to estimate overall survival (OS) and progression free survival (PFS), and the log-rank test was used to compare survival time. The independent prognostic factors were performed in multivariate analysis using the cox hazard model. *P* value <0.05 were considered to be significant. Graphical displays were prepared using Graph Pad Software (Graph Pad Software, Inc, La Jolla, CA) to show the distributions of expression.

Results

The upregulation of SIRT6 in lung squamous cell carcinoma

The characteristics of patients were shown in Table 1; there was no difference in terms of TNM stage, histology, age, gender and smoking history. Firstly, we detected the expression of *SIRT6* in 64 pairs of primary lung cancer and corresponding non-cancer tissues, the results revealed that the *SIRT6* was up-regulated by more than 2.81-fold in lung cancer compared with non-cancer tissues (Figure 1A; $P<0.001$). Whereas, there was no significant relationship between the *SIRT6* expression and age, tumor size, location, gender, smoking, and differentiation. Moreover, SIRT6 increased in L-SCC than L-AD (Figure 1B, and 1C; $P<0.01$); and advanced stage patients (stage III) had higher *SIRT6* expression than early stages (stage I and II) (Figure 1D, and 1E). In order to explore the relationship between the *SIRT6* expression and paclitaxel response, we compared the *SIRT6* expression between chemo-sensitive and chemo-resistant patients, and found that the *SIRT6* increased in patients who were resistant to chemotherapy (Table1, $P<0.001$).

Table 1

The characteristic of Patients and Relationships between Clinicopathological Factors and SIRT6 Expression

Variable	Patients(n)	SIRT6	*P*-value
Gender			
Male	30	2.23±0.07	
Female	34	2.33±0.15	0.517
Age			
<64 years	26	2.21±0.06	
≥64 years	38	2.32±0.12	0.477
Smoking			
Ever	43	2.25±0.07	
Never	21	2.35±0.20	0.529
Histology			
Adenocarcinoma	40	2.10±0.11	
Squamous cell carcinoma	24	2.58±0.06	0.0023
TNM stage			
I	25	1.73±0.03	
II	21	2.53±0.06	
III	18	3.16±0.05	<0.001
T factor			
T1	23	1.91±0.03	
T2	19	2.13±0.12	
T3	16	2.28±0.21	
T4	6	2.35±0.04	0.273
Lymph node metastasis			
Y	49	2.26±0.07	
N	15	2.34±0.25	0.656
Chemotherapy after operation			
Y	51	2.30±0.07	

N	13	2.21±0.27	0.642
Chemotherapy response			
Sensitive	39	1.83±0.04	
Resistance	12	3.22±0.05	<0.001
Recurrence			
Y	25	2.29±0.12	
N	39	0.27±0.07	0.906

Analysis also showed that *SIRT6* along with TNM stage was independent prognostic factor (Figure 1F-a, P<0.001) when Cox regression analysis with OS (overall survival) as the end point to identify independent prognostic factors among covariates including *SIRT6*, histological type, gender, and smoking history. Multivariate analysis with PFS (progression free survival) as the end point revealed that only *SIRT6* was an independent prognostic factor (Figure 1F-b, P<0.001).

SIRT6 promotes paclitaxel resistance via up-regulating TGF-β

We evaluated SIRT6 expression in the cytoplasm and nucleus of cells within the set of NSCLC tissues, and analyzed the correlation between SIRT6 cellular localization with clinicopathological factors. The associations between cytoplasmic SIRT6 expression in the NSCLC specimens and clinicopathological characteristics were shown in Table 2. IHC (Figure 2) and Immunofluorescence (Figure 3) showed that there was a correlation between SIRT6 location and TNM stage (*P*=0.024,). However, no difference was observed for other variables.

Table 2

Relationships Between Clinicopathological Factors and SIRT6 location

	Cytoplasm SIRT6		
	Low expression	High expression	
Variable	**n=29**	**n=35**	***P*-value**
Gender			
Male	13	17	
Female	16	18	0.81
Age			
<64 years	12	14	
≥64 years	17	21	0.91
Smoking			
Ever	20	23	
Never	9	12	0.78
Histology			
Adenocarcinoma	17	23	
Squamous cell carcinoma	12	12	0.56
TNM stage			
I	16	9	
II	9	12	
III	4	14	0.024
T factor			
T1	11	12	
T2	9	10	
T3	7	9	
T4	2	4	0.93
Lymph node metastasis			
Y	21	28	
N	8	7	0.47
Chemotherapy response			

Sensitive	16	23	
Resistance	5	7	0.96
Recurrence			
Y	15	10	
N	14	25	0.058

We also explored the molecular mechanism of SIRT6-induced chemoresistance, it has reported that “drug resistance originating from a TGF-β/FGF-2-driven EMT and its reversion in human lung adenocarcinoma cell lines harboring an EGFR mutation”; therefore, we determined whether TGF-β was the resistant protein that induced paclitaxel resistance through the SIRT6 upregulation? We detected the *SIRT6* and *TGF-β* expression in the *SIRT6* transduced and knocked out SW900 cell lines, and found that the *TGF-β* was consistent with *SIRT6* (Supplemental Figure 1), qRT-PCR and western blot also showed that SIRT6 and TGF-β improved in paclitaxel-resistant patients, whereas SIRT6 and TGF-β decreased in non-resistant ones (Figure 4A and 4C). Simultaneously, we detected the expression of SIRT6 and TGF-β in SW900-Taxol (paclitaxel resistant cell line) compared with SW900 cells. The results showed that SIRT6 and TGF-β were higher in SW900-Taxol than that in SW900 cell line (Figure 4B and 4D). In summary, we speculated that the paclitaxel resistance of L-SCC induced by up-regulated SIRT6 through increasing TGF-β, further molecular mechanism is still under study.

SAHA inhibits invasion and metastasis of lung squamous carcinoma cells

To study the effect of SAHA on cell proliferation, SW900 and SW900-Taxol were cultured in the presence of various SAHA concentrations. The results revealed that it could inhibit cell growth in a dose-dependent manner. The effective dose of SAHA that inhibited cell growth by 50% at 24 h was 8.6 μM for SW900, 12.0 μM for SW900-Taxol. The effective dose of paclitaxel that inhibited cell growth by 50% at 24 h was 28.5 μM for SW900, 37.2 μM for SW900-Taxol.

We investigated the effect of SAHA on the migration and invasion of lung squamous carcinoma cells. As a result, the inhibitory rates of migration and invasion on SW900 cells and SW900-Taxol cells were shown in Figure 5-I and Table 3, 4. Next, the viabilities of SW900 and SW900-Taxol treated with SAHA or paclitaxel were compared, as a result, combined treatments with SAHA and paclitaxel resulted in more reduction in cell viability compared with SAHA or paclitaxel treatment alone (Figure 5-II, $P<0.001$), which indicated that SAHA has re-sensitizing effect on paclitaxel-resistant lung squamous carcinoma cells.

Table 3
The inhibitory rates of migration and invasion on SW900 cells

	SAHA	Paclitaxel	SAHA + Paclitaxel	*P*
Migration	55%	47%	93%	<0.001
Invasion	71%	65%	82%	0.001

Table 4

The inhibitory rates of migration and invasion on SW900-Taxol cells

	SAHA	Paclitaxel	SAHA + Paclitaxel	*P*
Migration	48%	10%	89%	<0.001
Invasion	61%	9%	76%	<0.001

After treating with SAHA, western blot has detected the SIRT6 expression in these cell lines. Treatment with SAHA in SW900-Taxol cells (Figure 5-III) reduced SIRT6 expression more significantly than in SW900 cells (Figure 5-IV, $P<0.001$).

SAHA reverses paclitaxel resistance in lung squamous cell carcinoma through enhancing autophagy

In order to investigate the mechanism of re-sensitizing on paclitaxel-resistant cells, we examined the autophagy in SW900-Taxol cells. Compared with control and rapamycin (autophagic inducer) (Figure 6-I), SAHA induced more autophagosomes than paclitaxel (Figure 6-II, $P<0.010$). Combined treatments with SAHA and paclitaxel further enhanced the number of autophagosomes compared with SAHA alone, which chloroquine (autophagy inhibitor) could relieve it (Figure 6-III, $P<0.010$); so it suggested that SAHA could reverse the chemoresistance through enhancing autophagy.

Furthermore, the apoptotic changes in each group detected by the Annexin V-FITC/PI assay were consistent with the changes in apoptosis observed by flow cytometry. As shown in Figure 7-I, higher rates of apoptosis were induced in SW900-Taxol cells by SAHA combined with paclitaxel than SAHA alone ($P<0.01$).

To further validate the autophagic flux, different autophagy markers were analyzed. As a result, LC3 was the highest when treated with SAHA combined with paclitaxel ($P<0.001$), whereas, the degradation protein of p62, an adaptor protein which served as an autophagy receptor targeting ubiquitin proteins to

autophagosomes for degradation; decreased significantly (P<0.001), indicating an enhanced autophagic flux (Figure 7-II).

Discussion

Lung adenocarcinoma patients have more therapeutic choices, such as chemotherapy and epidermal growth factor receptor tyrosine kinase inhibitors (EGFR-TKIs); not only the overall survival is appreciable, but also the side effect is less. However, the treatment options for L-SCC patients are limited, some L-SCC patients are intrinsically resistant to chemotherapy.[19] In fact, all patients, including initial responders, rapidly develop chemoresistance, which, in the absence of alternative therapies, leads to 5-year survival rate less than 15%.[20] Therefore, better understanding the molecular determinants is critically important to overcome the chemoresistance responsible for the dismal survival.

Tumor metastasis is characterized by rapidly proliferating and drug resistance. An increasing evidence suggested that the survival of a small portion of cells with stem-like properties may be responsible for tumor recurrences after initial response to chemotherapy.[21] TGF-β was a potent inducer of an epithelial-to-mesenchymal transition (EMT) in mammary cells, and this transformation has been associated with acquisition of tumor stem-like properties.[22,23] TGF-β ligands, enriched in tumor microenvironment, could be produced by tumor cells or by tumor-associated stromal and immune cells. These data suggested the possibility that TGF-β pathway was involved in acquired chemoresistance. Carlos L. Arteaga *et al*. revealed that TGF-β inhibition enhanced chemotherapy action against triple-negative breast cancer;[24] Yhun Yhong Sheen *et al*. also reported that combinatorial TGF-β attenuation with paclitaxel inhibited the EMT and breast cancer stem-like cells.[25] Based on above studies, we speculated that: 1) the EMT induced by TGF-β was closely associated with tumor metastasis and acquired chemoresistance; 2) blocking TGF-β pathway would enhance the chemotherapeutic effect; 3) combined paclitaxel with TGF-β pathway inhibitors have a synergistic effect. These findings have provided guidance for the therapy of chemoresistance induced by TGF-β improvement.

However, which gene to regulate the TGF-β pathway function? It is reported that SIRT6 inhibited EMT during idiopathic pulmonary fibrosis (IPF) via inactivating TGF-β1/Smad3 signaling,[26] and others have discovered that *SIRT6* suppressed cell proliferation through inhibiting Twist1 in the NSCLC.[27] Whereas, in present study, we reported that the upregulated *SIRT6* induced paclitaxel-resistance via TGF-β pathway, and the improvement of *SIRT6* predicted poor prognosis in L-SCC patients. Therefore, we speculated that: 1) *SIRT6* might regulate the TGF-β expression; 2) the regulatory role of SIRT6 was in contradiction with previous study. The possible reasons are as follows: 1) the microenvironments in IFP and lung cancer were distinct; resulting in that *SIRT6* might play different function; just as has revealed that *SIRT6* suppresses pancreatic cancer through controling Lin28b, and *SIRT6* was a tumor suppressor that controled cancer metabolism.[8] Although *SIRT6* has been shown to be a tumor suppressor in pancreatic cancer; some researchers have demonstrated that the upregulated *SIRT6* predicted poor prognosis and promoted the NSCLC metastasis via ERK1/2/MMP9 pathway.[28] It also has reported that *SIRT6* was

associated with poor prognosis and chemosensitivity in the NSCLC patients,[29] all these findings indicated that *SIRT6* was one oncogene in lung cancer; which were consistent with us, and *SIRT6* played diverse epigenetic role on different pathways and metabolic processes, and the obvious divergence has existed in EMT-mediated tumor process and drug resistance.

Next, we intended to determine the therapeutic effect of SAHA alone or combined with paclitaxel on lung cancer. As a result, we found that SAHA has significant effect on paclitaxel-resistant L-SCC and re-sensitized the resistant cells when combined with paclitaxel. However, it has been demonstrated that in *vitro*, SAHA alone decreased viability and increased apoptosis similarly to paclitaxel. In *vivo*, paclitaxel followed by SAHA and paclitaxel alone increased survival compared with SAHA alone or SAHA followed by paclitaxel.[30] This suggested adding SAHA to ovarian cancer chemotherapy could increase the efficacy and the agents sequencing was important. In addition, they found that the ef□cacy of combination and sequence of SAHA and paclitaxel administration were cell line dependent, suggesting that the responses varied based on tumor speci□c characteristics.

In several cancers, it has shown that HDACi lead to autophagy induction, whereas, whether it was protective or toxic for cancer cells has been depending on the types of cancer.[31] Therefore, we examined whether the combined treatments enhanced the autophagy and what was the role of autophagy in the synergistic cytotoxic effect. We demonstrated that the combined treatment depended on autophagy and that inhibition of autophagy resulted in reduced apoptosis and cell death. The interplay between autophagy and apoptosis was complicated,[32] however, it was clear that the autophagy and apoptosis were cross-talk. Under certain conditions, the activation of autophagy inhibited apoptosis, in other condition, autophagy activated it. That was, apoptosis could be induced directly by the treatments or indirectly via autophagy induced by the treatments. Our results showed that the autophagy acted as a cell death mechanism of combined treatment, because the autophagy inhibition brought about a decrease in cell death.

In present study, there were several limitations requiring further exploring: 1) absence of SIRT6 lentivirus interference in cell experiments, so the regulatory mechanism of SIRT6 needed to be validated in-depth; 2) there may be many other mechanism in reversing drug resistance except for autophagy; 3) the number of patients needed to expanded and the follow-up time to be extended.

Declarations

Acknowledgments

Research projects of Shanghai health and Planning Commission (No. 201740015) funded this work.

Conflict of Interest Disclosure Statement

There is no conflict of interest for any of the authors in any aspects of the article.

References

1. Liao BC, Shao YY, Chen HM, et al. Comparative effectiveness of first-line platinum-based chemotherapy regimens for advanced lung squamous cell carcinoma. *Clin Lung Cancer*. 2015;16(2):137-143. doi: 10.1016/j.cllc.2014.09.004.
2. Kuribayashi K, Funaguchi N, Nakano T. Chemotherapy for advanced non-small cell lung cancer with a focus on squamous cell carcinoma. *J Cancer Res Ther*. 2016;12(2):528-534. doi: 10.4103/0973-1482.174185.
3. Finkel T, Deng CX, Mostoslavsky R. Recent progress in the biology and physiology of sirtuins. *Nature*. 2009;460(7255):587-591. doi: 10.1038/nature08197.
4. Mahlknecht U, Ho AD, Voelter-Mahlknecht S. Chromosomal organization and fluorescence in situ hybridization of the human Sirtuin 6 gene. *Int J Oncol*. 2006;28(2):447-456.
5. Voelter-Mahlknecht S, Letzel S, Mahlknecht U. Fluorescence in situ hybridization and chromosomal organization of the human Sirtuin 7 gene. *Int J Oncol*. 2006;28(4):899-908.
6. Liu Y, Xie QR, Wang B, et al. Inhibition of SIRT6 in prostate cancer reduces cell viability and increases sensitivity to chemotherapeutics. *Protein Cell*. 2013;4(9):702-710. doi: 10.1007/s13238-013-3054-5.
7. Ming M, Han W, Zhao B, et al. SIRT6 promotes COX-2 expression and acts as an oncogene in skin cancer. *Cancer Res*. 2014;74(20):5925-5933. doi: 10.1158/0008-5472.CAN-14-1308.
8. Kugel S, Sebastián C, Fitamant J, et al. SIRT6 Suppresses Pancreatic Cancer through Control of Lin28b. *Cell*. 2016;165(6):1401-1415. doi: 10.1016/j.cell.2016.04.033.
9. Ran LK, Chen Y, Zhang ZZ, et al. SIRT6 Overexpression Potentiates Apoptosis Evasion in Hepatocellular Carcinoma via BCL2-Associated X Protein-Dependent Apoptotic Pathway. *Clin Cancer Res*. 2016;22(13):3372-3382. doi: 10.1158/1078-0432.CCR-15-1638.
10. Zhang ZG, Qin CY. Sirt6 suppresses hepatocellular carcinoma cell growth via inhibiting the extracellular signal-regulated kinase signaling pathway. *Mol Med Rep*. 2014;9(3):882-888. doi: 10.3892/mmr.2013.1879.
11. Rizzo A, Iachettini S, Salvati E, et al. SIRT6 interacts with TRF2 and promotes its degradation in response to DNA damage. *Nucleic Acids Res*. 2017;45(4):1820-1834. doi: 10.1093/nar/gkw1202.
12. Choe M, Brusgard JL, Chumsri S, et al. The RUNX2 Transcription Factor Negatively Regulates SIRT6 Expression to Alter Glucose Metabolism in Breast Cancer Cells. *J Cell Biochem*. 2015;116(10):2210-2226. doi: 10.1002/jcb.25171.
13. Khongkow M, Olmos Y, Gong C, et al. SIRT6 modulates paclitaxel and epirubicin resistance and survival in breast cancer. *Carcinogenesis*. 2013;34(7):1476-1486. doi: 10.1093/carcin/bgt098.
14. Cai Y, Sheng ZY, Liang SX. Radiosensitization effect of overexpression of adenovirus-mediated SIRT6 on A549 non-small cell lung cancer cells. *Asian Pac J Cancer Prev*. 2014;15(17):7297-7301. doi: 10.7314/apjcp.2014.15.17.7297.
15. Tordera V, Sendra R, Pérez-Ortín JE. The role of histones and their modifications in the informative content of chromatin. *Experientia*. 1993;49(9):780-788.

16. Owonikoko TK, Ramalingam SS, Kanterewicz B, et al. Vorinostat increases carboplatin and paclitaxel activity in non-small-cell lung cancer cells. *Int J Cancer*. 2010;126(3):743-755. doi: 10.1002/ijc.24759.
17. Dietrich CS, Greenberg VL, DeSimone CP, et al. Suberoylanilide hydroxamic acid (SAHA) potentiates paclitaxel-induced apoptosis in ovarian cancer cell lines. *Gynecol Oncol*. 2010;116(1):126-130. doi: 10.1016/j.ygyno.2009.09.039.
18. Dowdy SC, Jiang S, Zhou XC, et al. Histone deacetylase inhibitors and paclitaxel cause synergistic effects on apoptosis and microtubule stabilization in papillary serous endometrial cancer cells. *Mol Cancer Ther*. 2006;5(11):2767-2776.
19. Shtivelman E, Hensing T, Simon GR, et al. Molecular pathways and therapeutic targets in lung cancer. *Oncotarget*. 2014;5(6):1392-1433. doi: 10.18632/oncotarget.1891.
20. Jadus MR, Natividad J, Mai A, et al. Lung cancer: a classic example of tumor escape and progression while providing opportunities for immunological intervention. *Clin Dev Immunol*. 2012;2012:160724. doi: 10.1155/2012/160724.
21. Herpel E, Jensen K, Muley T, et al. The cancer stem cell antigens CD133, BCRP1/ABCG2 and CD117/c-KIT are not associated with prognosis in resected early-stage non-small cell lung cancer. *Anticancer Res*. 2011;31(12):4491-4500.
22. Mirza S, Jain N, Rawal R. Evidence for circulating cancer stem-like cells and epithelial-mesenchymal transition phenotype in the pleurospheres derived from lung adenocarcinoma using liquid biopsy. *Tumour Biol*. 2017;39(3):1010428317695915. doi: 10.1177/1010428317695915.
23. Li X, Han J, Zhu H, Peng L, Chen Z. miR-181b-5p mediates TGF-β1-induced epithelial-to-mesenchymal transition in non-small cell lung cancer stem-like cells derived from lung adenocarcinoma A549 cells. *Int J Oncol*. 2017;51(1):158-168. doi: 10.3892/ijo.2017.4007.
24. Bhola NE, Balko JM, Dugger TC, et al. TGF-β inhibition enhances chemotherapy action against triple-negative breast cancer. *J Clin Invest*. 2013;123(3):1348-1358. doi: 10.1172/JCI65416.
25. Park SY, Kim MJ, Park SA, et al. Combinatorial TGF-β attenuation with paclitaxel inhibits the epithelial-to-mesenchymal transition and breast cancer stem-like cells. *Oncotarget*. 2015;6(35):37526-37543. doi: 10.18632/oncotarget.6063.
26. Tian K, Chen P, Liu Z, et al. Sirtuin 6 inhibits epithelial to mesenchymal transition during idiopathic pulmonary fibrosis via inactivating TGF-β1/Smad3 signaling. *Oncotarget*. 2017;8(37):61011-61024. doi: 10.18632/oncotarget.17723.
27. Han Z, Liu L, Liu Y, Li S. Sirtuin SIRT6 suppresses cell proliferation through inhibition of Twist1 expression in non-small cell lung cancer. *Int J Clin Exp Pathol*. 2014;7(8):4774-4781.
28. Bai L, Lin G, Sun L, et al. Upregulation of SIRT6 predicts poor prognosis and promotes metastasis of non-small cell lung cancer via the ERK1/2/MMP9 pathway. *Oncotarget*. 2016;7(26):40377-40386. doi: 10.18632/oncotarget.9750.
29. Azuma Y, Yokobori T, Mogi A, et al. SIRT6 expression is associated with poor prognosis and chemosensitivity in patients with non-small cell lung cancer. *J Surg Oncol*. 2015;112(2):231-237. doi:

10.1002/jso.23975.

30. Cooper AL, Greenberg VL, Lancaster PS, et al. In vitro and in vivo histone deacetylase inhibitor therapy with suberoylanilide hydroxamic acid (SAHA) and paclitaxel in ovarian cancer. *Gynecol Oncol*. 2007;104(3):596-601.
31. Lin KT, Wang YW, Chen CT, et al. HDAC inhibitors augmented cell migration and metastasis through induction of PKCs leading to identification of low toxicity modalities for combination cancer therapy. *Clin Cancer Res*. 2012;18(17):4691-4701. doi: 10.1158/1078-0432.CCR-12-0633.
32. Walsh CM, Edinger AL. The complex interplay between autophagy, apoptosis, and necrotic signals promotes T-cell homeostasis. *Immunol Rev*. 2010;236. doi: 10.1111/j.1600-065X.2010.00919.x.

Figures

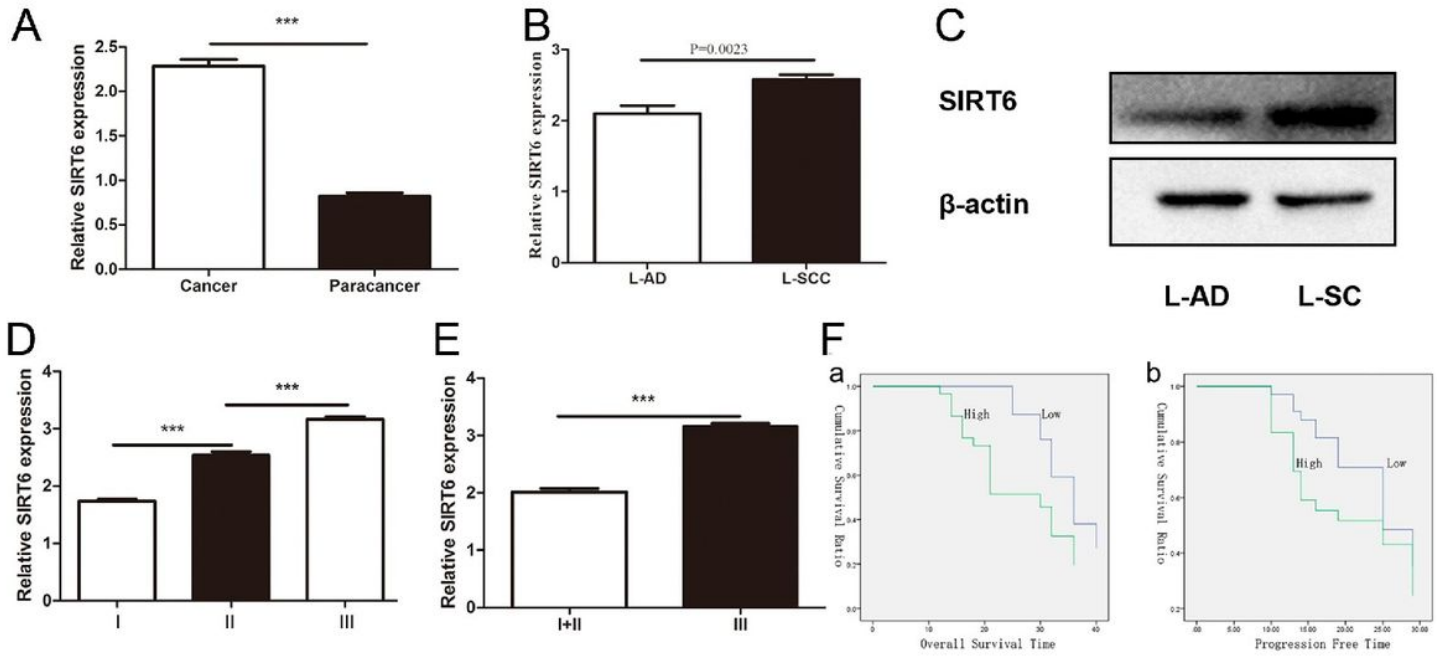

Figure 1

A. *SIRT6* was up-regulated in lung cancer compared with non-tumorous tissues (P<0.001); B, C. showed that SIRT6 increased significantly in L-SC than L-AD (P<0.01); D, E. showed that *SIRT6* expression increased with TNM stage.

F. showed that *SIRT6* was an independent prognostic factor (P<0.001); 1F-a: OS as the end point; 1F-b: PFS as the end point.

Figure 2

IHC showed the SIRT6 location; A. Para-cancer; B. IA stage, High Nuclear expression; C. IIB stage, Cytoplasm and nucleus co-expression; D. III stage, Cytoplasm expression.

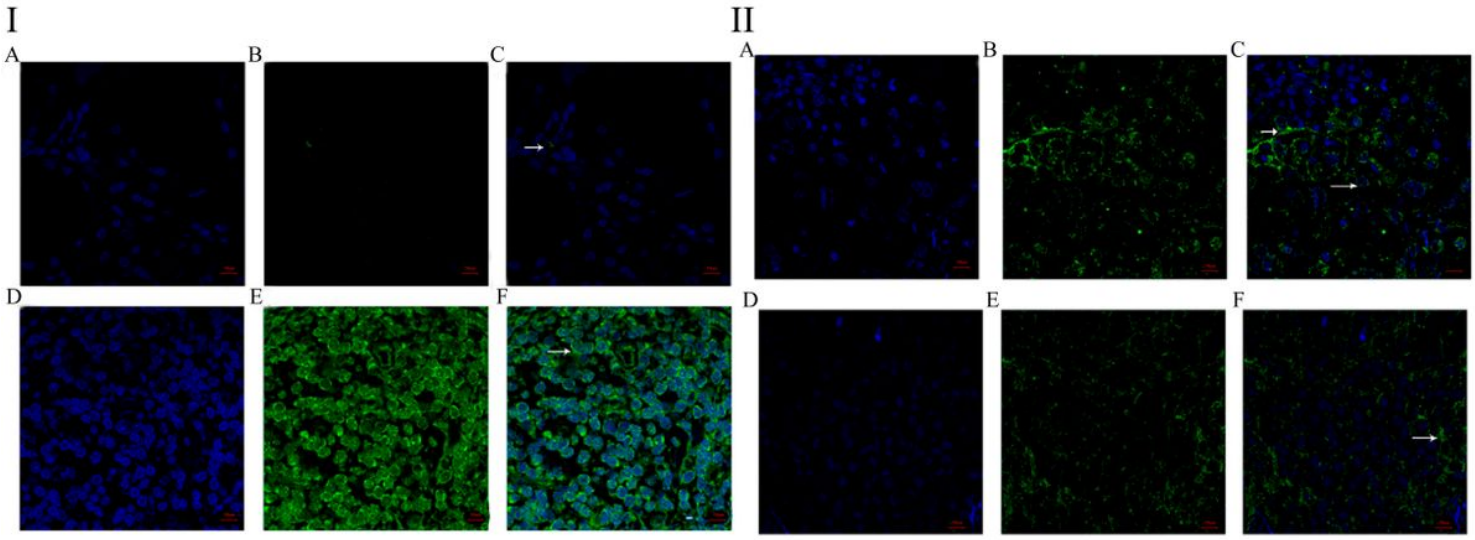

Figure 3

3-I: Immunofluorescence showed the SIRT6 location; A, B, C. Para-cancer; D, E, F. IA stage, High Nuclear expression. **3-II:** Immunofluorescence showed the SIRT6 location; A, B, C. IIB stage Cytoplasm and nucleus co-expression; D, E, F. III stage, Cytoplasm expression.

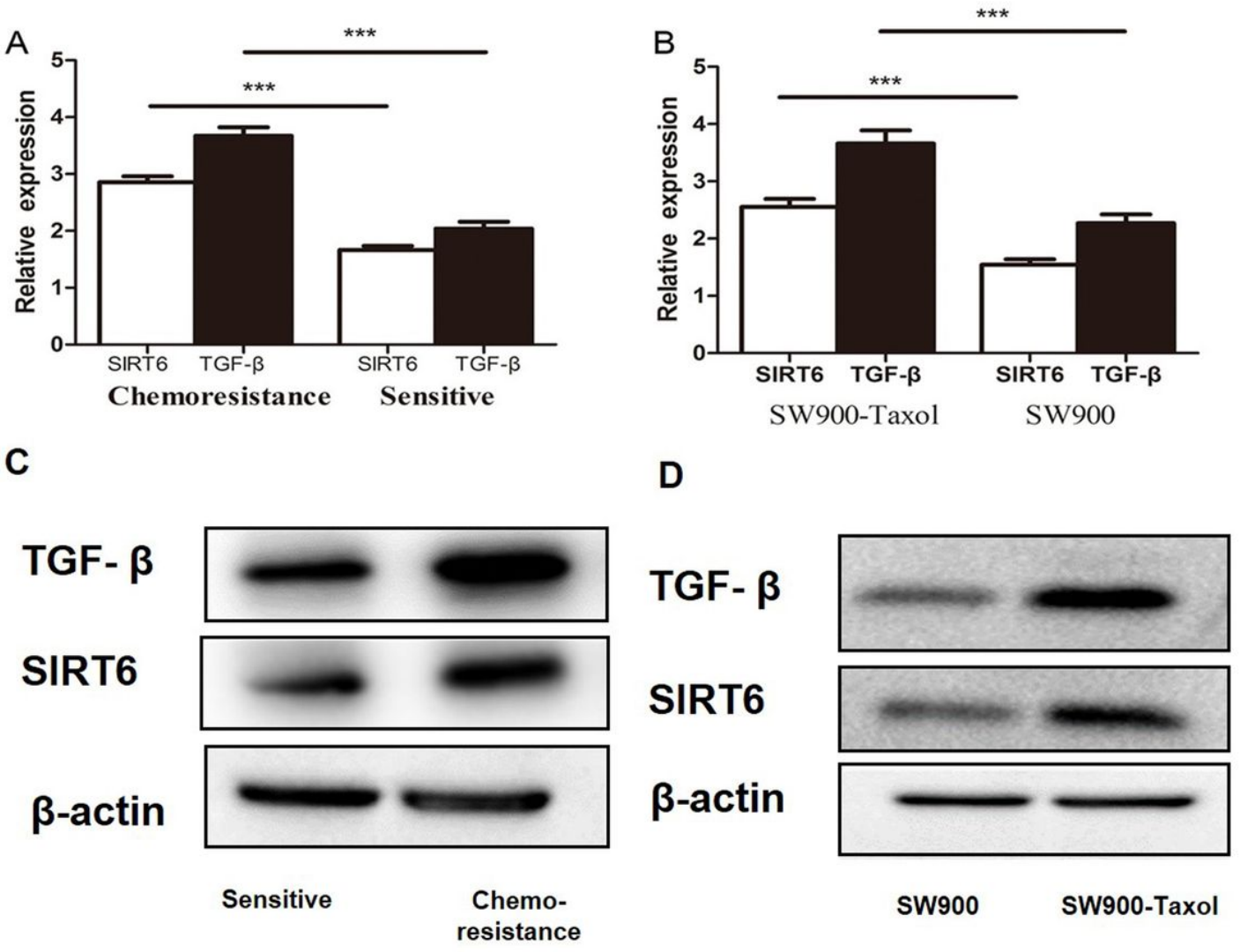

Figure 4

A and C. qPCR and Western blot showed that *SIRT6* and *TGF-β* improved in paclitaxel-resistant patients, decreased in non-resistance. B and D. *SIRT6* and *TGF-β* were higher in SW900-Taxol cell lines than that in SW900.

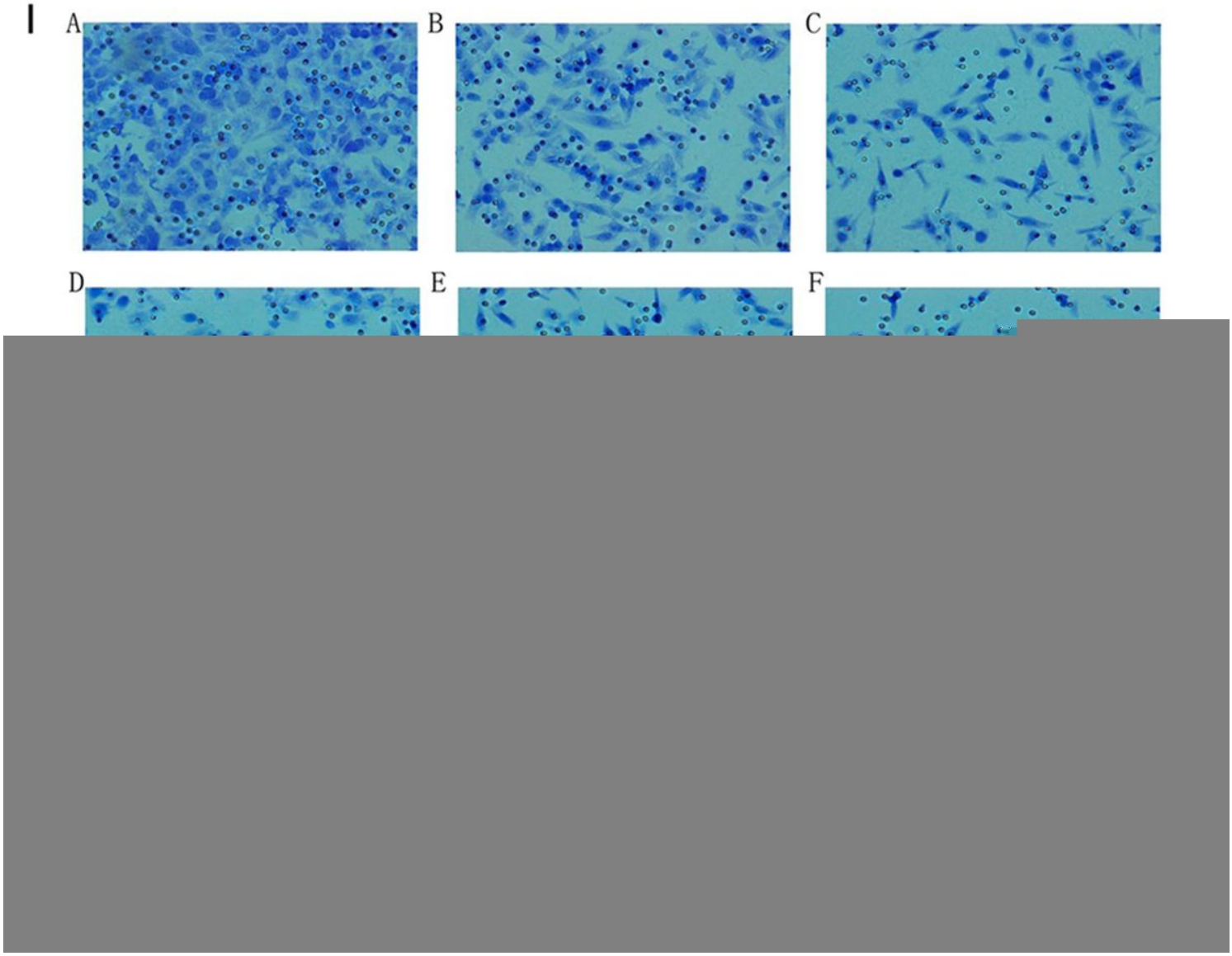

Figure 5

SAHA inhibits cell migration and invasion on SW900 cells and SW900-Taxol cells; I-A, B, C. SAHA inhibits SW900 cells; I-D, E, F. SAHA inhibits SW900-Taxol cells. II. SAHA, paclitaxel, SAHA combined with paclitaxel inhibit the viability of SW900 cells and SW900-Taxol cells. III. Western blot showed SAHA reduced SIRT6 expression of SW900-Taxol cells in a dose dependent fashion; IV. Western blot showed SAHA reduced SIRT6 expression of SW90 cells.

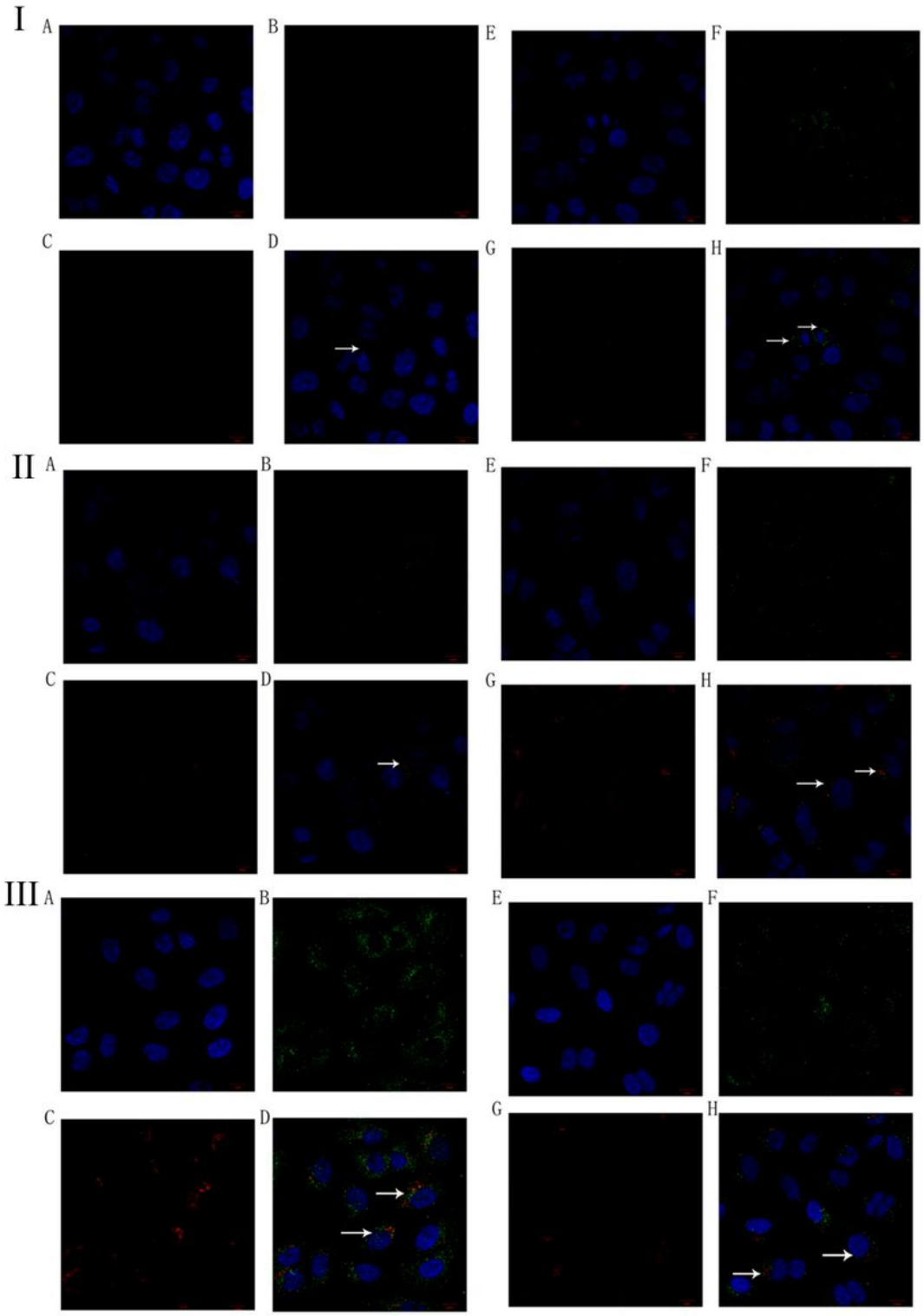

Figure 6

Autophagy changes under different treatments for SW900-Taxol cells. I-A, B, C, D. Serum-free medium Starvation for 24h; I-E, F, G, H. Rapamycin (30 umol/L) for 24h; II- A, B, C, D. Paclitaxel (37.2 umol/L) for 24h; II-E, F, G, H. SAHA (12 umol/L) for 24h; III-A, B, C, D. SAHA combined with paclitaxel for 24h; III-E, F, G, H. SAHA combined with paclitaxel plus chloroquine treatment for 24h.

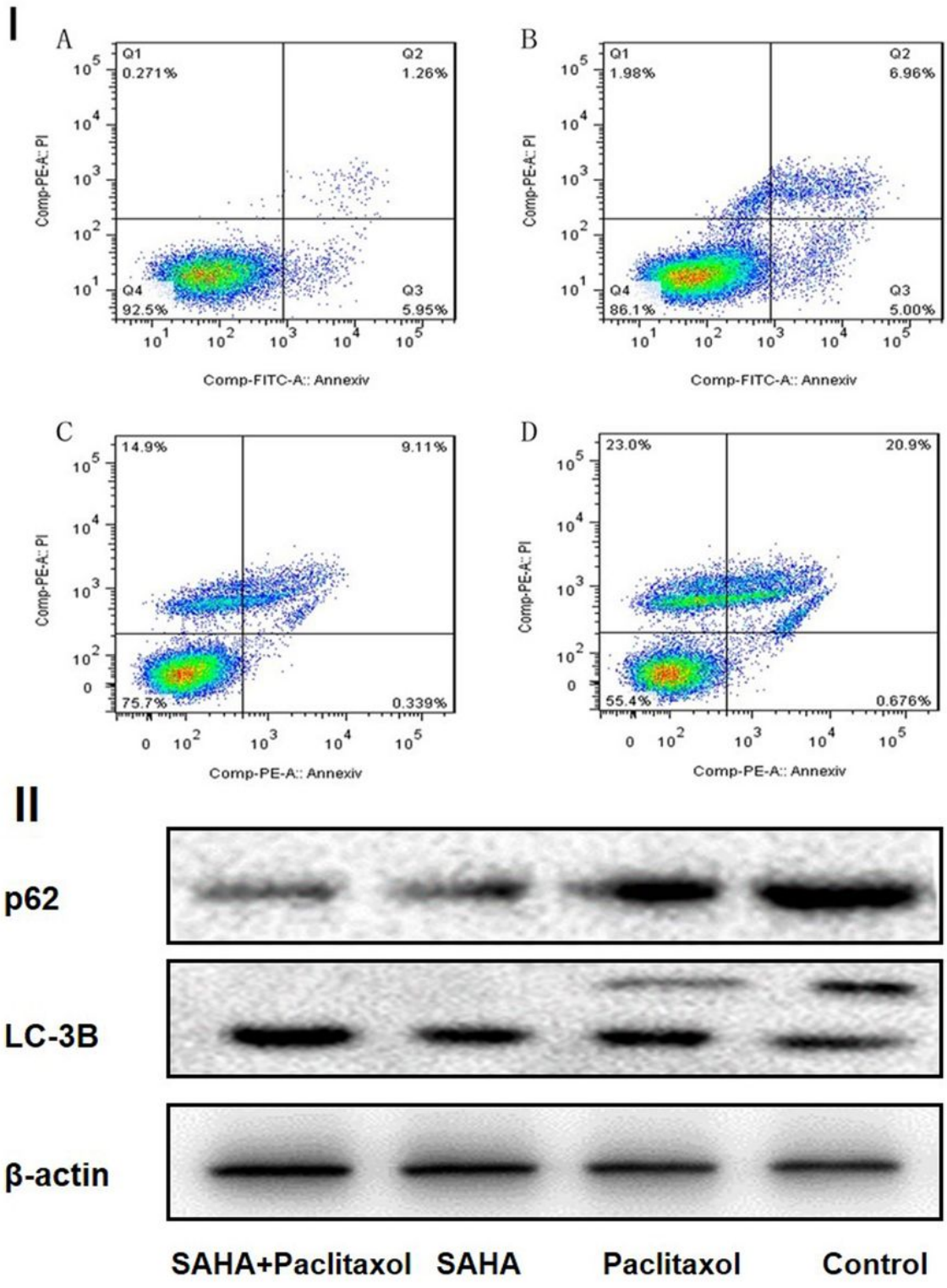

Figure 7

The apoptotic changes in each group; I-A. Control; I-B. Paclitaxel treatment; I-C. SAHA treatment; I-D. SAHA combined with paclitaxel treatment.

II. Western blot showed that autophagy markers flux under different treatments.

Supplementary Files

This is a list of supplementary files associated with this preprint. Click to download.

- SupplementalFigure1.docx